JGR Oceans

RESEARCH ARTICLE
10.1029/2020JC016124

Evaluation of Data-Based Estimates of Anthropogenic Carbon in the Arctic Ocean

J. Terhaar[1,2], T. Tanhua[3], T. Stöven[3], J. C. Orr[1], and L. Bopp[4]

[1]Laboratoire des Sciences du Climat et de l'Environnement, LSCE/IPSL, CEA-CNRS-UVSQ, Université Paris-Saclay, Gif-sur-Yvette, France, [2]Biogeochemistry and Earth System Modelling, Department of Geoscience, Environment and Society, Université Libre de Bruxelles, Bruxelles, Belgium, [3]GEOMAR Helmholtz Centre for Ocean Research Kiel, Kiel, Germany, [4]Laboratoire de Météorologie Dynamique, LMD/IPSL, Ecole Normale Supérieure / PSL Université, CNRS, Ecole Polytechnique, Sorbonne Université, Paris, France

Abstract The Arctic Ocean is particularly vulnerable to ocean acidification, a process that is mainly driven by the uptake of anthropogenic carbon (C_{ant}) from the atmosphere. Although C_{ant} concentrations cannot be measured directly in the ocean, they have been estimated using data-based methods such as the transient time distribution (TTD) approach, which characterizes the ventilation of water masses with inert transient tracers, such as CFC-12. Here, we evaluate the TTD approach in the Arctic Ocean using an eddying ocean model as a test bed. When the TTD approach is applied to simulated CFC-12 in that model, it underestimates the same model's directly simulated C_{ant} concentrations by up to 12%, a bias that stems from its idealized assumption of gas equilibrium between atmosphere and surface water, both for CFC-12 and anthropogenic CO_2. Unlike the idealized assumption, the simulated partial pressure of CFC-12 (pCFC-12) in Arctic surface waters is undersaturated relative to that in the atmosphere in regions and times of deep-water formation, while the simulated equivalent for C_{ant} is supersaturated. After accounting for the TTD approach's negative bias, the total amount of C_{ant} in the Arctic Ocean in 2005 increases by 8% to 3.3 ± 0.3 Pg C. By combining the adjusted TTD approach with scenarios of future atmospheric CO_2, it is estimated that all Arctic waters, from surface to depth, would become corrosive to aragonite by the middle of the next century even if atmospheric CO_2 could be stabilized at 540 ppm.

Key Points:
- The amount of anthropogenic carbon in the Arctic Ocean appears to be underestimated by 7–12%
- A refined approach yields a new estimate of 3.3 ± 0.3 Pg C for year 2005
- All Arctic Ocean waters become corrosive to aragonite if atmospheric CO2 is held at 540 ppm

Supporting Information:
- Supporting Information S1

Correspondence to:
J. Terhaar,
jens.terhaar@climate.unibe.ch

Citation:
Terhaar, J., Tanhua, T., Stöven, T., Orr, J. C., & Bopp, L. (2020). Evaluation of data-based estimates of anthropogenic carbon in the Arctic Ocean. *Journal of Geophysical Research: Oceans*, *125*, e2020JC016124. https://doi.org/10.1029/2020JC016124

Received 29 JAN 2020
Accepted 7 MAY 2020
Accepted article online 11 MAY 2020

This article was prematurely published without the authors' corrections. Corrections were made on 28 June 2020, to incorporate the authors' changes.

1. Introduction

Ocean uptake of anthropogenic carbon (C_{ant}) drives reductions in ocean pH and carbonate ion concentration, the latter of which reduces the calcium carbonate ($CaCO_3$) saturation state (Orr et al., 2005). Surface waters in the high latitudes have naturally lower $CaCO_3$ saturation states; hence, as atmospheric CO_2 climbs, they are more susceptible to reaching saturation states below which they become undersaturated with respect to aragonite, a metastable form of $CaCO_3$ (Orr et al., 2005; Steinacher et al., 2009). Unlike in almost all other regions, surface waters in the Arctic Ocean are already partly undersaturated with respect to aragonite particularly near river mouths because of lower alkalinity freshwater input (Chierici & Fransson, 2009; Mathis et al., 2015; Semiletov et al., 2016). The Arctic Ocean's annual-mean conditions are projected to become entirely undersaturated with respect to aragonite by 2080 under the SRES A2 scenario (Steinacher et al., 2009).

The Arctic's aragonite saturation horizon (ASH), above which waters are supersaturated with respect to aragonite and below which they are undersaturated, is located at around 1,900 m (Anderson et al., 2010). The Arctic ASH is projected to shoal by ~100 m during the 21st century based on a coupled carbon-climate model forced under the SRES A2 scenario (Steinacher et al., 2009). The same model projects that the aragonite undersaturation in surface waters will propagate downwards rapidly, merging with the shoaling ASH at about 1,800 m by the end of the century. Conversely, a data-based approach that imposes exponentially increasing atmospheric CO_2 suggests that the deep ASH will shoal by much more (~900 m) and will merge with the deepening undersaturation from the surface at about 1,000 m by the end of the century (Anderson et al., 2010).

The main driver of acidification in the open ocean is the increase in atmospheric CO_2 during the industrial era and the resulting uptake of C_{ant} by the ocean. Although this absorbed C_{ant} cannot be measured directly,

it has been estimated from other oceanographic data by various methods, such as the transit-time distribution (TTD) approach (Khatiwala et al., 2013; Waugh et al., 2006). For instance, the inverse Gaussian-TTD (IG-TTD) method, a specific solution of the TTD framework, aims to constrain the invasion of C_{ant} into the interior ocean by using observations of transient tracers such as CFC-12, the tritium-helium pair ($^3H/^3He$), and SF_6 (Hall et al., 2002; Waugh et al., 2004). With surface boundary conditions of the chosen tracer (e.g., CFC-12) as well as subsurface measurements of the same tracer, temperature (T), and salinity (S), the mean age of the water parcel can be determined by the IG-TTD approach. The resulting mean age is then used in combination with the atmospheric CO_2 history to estimate the C_{ant} concentration in the respective water parcel.

The TTD approach was first applied to the global ocean by Waugh et al. (2006), who estimated a global ocean C_{ant} uptake of 134 Pg C in 1994. Waugh et al. did not apply the TTD approach in the Arctic because tracer observations there were sparse. Later, with the advent of more tracer observations, Tanhua et al. (2009) applied the TTD method to the Arctic Ocean, estimating that it contained 2.5–3.3 Pg of anthropogenic carbon in 2005. From the TTD estimates of C_{ant} concentrations along the 2005 Beringia section, Anderson et al. (2010) estimated that the Arctic Ocean's average depth of the ASH had shoaled by ~190 m during the industrial era.

The skill of related data-based approaches has been tested in general ocean circulation models (Matear et al., 2003; Matsumoto & Gruber, 2005). In a similar fashion, the TTD approach can be applied to simulated CFC-12 concentrations to obtain a TTD-based estimate of C_{ant} in the same model as where C_{ant} is simulated directly (reference C_{ant}), for example, using the perturbation approach for C_{ant} from Sarmiento et al. (1992). The first such TTD evaluation by Waugh et al. (2006) indicated that the TTD-derived C_{ant} is similar to the directly simulated C_{ant} reference in all modeled ocean regions except for the Southern Ocean. The issue in the Southern Ocean stems from its upwelled deeper waters, which are impoverished in CFC-12 and C_{ant} and spend only about 4 months at the surface before being subducted into the ocean interior (Weiss et al., 1979). Although that period is sufficient for air-sea equilibration of CFC-12, such is not the case for C_{ant} whose complete air-sea equilibration takes longer (Broecker & Peng, 1974). Conversely, the TTD approach assumes equilibrium between the atmosphere and surface ocean for both C_{ant} and CFC-12. Hence, that data-based approach systematically overestimates C_{ant} in the Southern Ocean (Matear et al., 2003; Waugh et al., 2006).

In the Arctic Ocean, differences between C_{ant} and CFC-12 in terms of surface-water saturation relative to the atmosphere are also thought to cause biases in the TTD-based C_{ant} estimates. But in that region, the sign and magnitude of these biases have not been evaluated (Tanhua et al., 2009). Recently, Rajasakaren et al. (2019) revised upward the C_{ant} inventory estimate for the Arctic Ocean to 3.6 Pg C in 2005 after accounting for the undersaturation of surface-water CFC-12 relative to the atmosphere. However, the associated uncertainty is large. Moreover, they did not account for the related air-sea disequilibrium for C_{ant}, which could be larger in magnitude owing to its longer air-sea equilibration time. They also changed other parameters of the TTD approach, making it impossible to isolate the effect of differences in surface saturation of CFC-12. In this study, our goals are (1) to evaluate the TTD method in the Arctic Ocean with an ocean model and (2) to use results from that assessment to adjust the existing TTD data-based estimate of the Arctic C_{ant} inventory (Tanhua et al., 2009).

2. Methods

2.1. Arctic Ocean and Its Water Masses

The boundaries of the Arctic Ocean are defined following Bates and Mathis (2009), that is, at the Fram Strait, the Barents Sea Opening, the Bering Strait, and the Canadian Arctic Archipelago (between Smith Sound and Baffin Bay).

Arctic Ocean water masses are also defined based on previous studies (Table S1). The Pacific Water (PW) is divided into (1) the Summer Pacific Water (SPW), having temperatures between −1.0°C and 0.4°C and salinities between 31 and 33 (Bourgain et al., 2013; Steele et al., 2004; Woodgate et al., 2010), and (2) the Winter Pacific Water (WPW), having temperatures below −1.4°C and salinities above 32.4 (Pickart et al., 2005). Water from the Atlantic Ocean splits into two branches. The first branch enters the Arctic Ocean through the Fram Strait at intermediate depths and is generally warmer than 0°C and saltier than 34 (Woodgate, 2013). Being disconnected from the surface, it tends to conserve these characteristics and is thus named Atlantic Water (AW). The second branch enters the Arctic Ocean through the Barents Sea Opening. Being

mainly located at the surface, it cools to less than 0°C and its salinity increases to values above 34.6 owing to brine rejection (Midttun, 1985). Consequently, the density of this water mass increases, which drives its descent into the deep Arctic Ocean basins through the St Anna Trough (Gammelsrød et al., 2009; Schauer et al., 2002; Smedsrud et al., 2013). Water masses from this second Atlantic branch are named Barents Sea Water (BSW).

2.2. Ocean Model

In this study, we used the global ocean circulation model Nucleus for European Modeling of the Ocean—version 3.2 (NEMO-v3.2) (Madec, 2008) combined with a single-tracer perturbation approach to simulate C_{ant} (Lachkar et al., 2007; Palmiéri et al., 2015; Sarmiento et al., 1992). This approach is computationally less expensive than a full biogeochemical model, which facilitates running the physical model at higher resolution. The atmospheric CO_2 forcing for years 1765–1869 comes from Meinshausen et al. (2017) while that for years 1870–2012 is from Le Quéré et al. (2015). To calculate the anthropogenic change in surface-ocean partial pressure of CO_2 (pCO_2), referred to as δpCO_2, the perturbation approach exploits the nearly linear relationship between δpCO_2 and the ratio between the corresponding perturbation in total dissolved inorganic carbon (δC_T) and δpCO_2 (Sarmiento et al., 1992)

$$\frac{\delta pCO_2}{\delta C_T} = z_0 + z_1 \delta pCO_2, \tag{1}$$

where z_0 and z_1 are each quadratic functions of surface temperature (° C):

$$z_0 = a_0 + a_1 T + a_2 T^2, \tag{2}$$

$$z_1 = b_0 + b_1 T + b_2 T^2. \tag{3}$$

The fitted parameters a_0, a_1, a_2, b_0, b_1, and b_2 are taken from Terhaar et al. (2019, Table 4) and were calculated with the K_1 and K_2 dissociation constants from Lueker et al. (2000), the dissociation constant for boric acid from Dickson (1990), and the total boron-to-salinity ratio from Uppström (1974). For perturbations in atmospheric CO_2 of up to 280 ppm (a doubling of the preindustrial level), the relationship between $\delta pCO_2/\delta C_T$ and δpCO_2 is essentially linear under the assumption of constant total alkalinity A_T ($2300 \mu mol kg^{-1}$) and salinity (35). Hence, it depends only on surface ocean temperature. Rearranging (1) yields

$$\delta pCO_2 = \frac{z_0 \delta C_T}{1 - z_1 \delta C_T}, \tag{4}$$

the equation by which simulated surface temperature and δC_T are used to compute surface δpCO_2, as needed to compute the air-sea C_{ant} flux:

$$F_{C_{ant}} = \alpha k_w (\delta pCO_2^{atm} - \delta pCO_2^{oce}), \tag{5}$$

where α is the solubility of CO_2 (Weiss, 1974), k_w is the gas transfer velocity (Wanninkhof, 1992), and δpCO_2^{atm} and δpCO_2^{oce} are the anthropogenic changes in partial pressure in the atmosphere and the surface ocean, respectively. For brevity, δpCO_2^{oce} is usually indicated here as δpCO_2. The experimentally derived gas transfer velocity implicitly accounts for some effects of bubbles on the air-sea C_{ant} flux, but not the direct effect of bubbles on gas saturation anomalies from bubble dissolution (Hamme et al., 2017). While bubbles enhance the gas saturation of less soluble gases, for example, O_2 (Atamanchuk et al., 2020) and SF_6 (Stöven et al., 2015), they have little effect on the saturation of CO_2 and CFC-12, which are more soluble (Hamme et al., 2017; Stöven et al., 2015). Once transferred to the ocean, C_{ant} was treated as a passive tracer with no internal sources nor sinks.

Despite these approximations, the simulated Arctic Ocean C_{ant} inventory (total mass in the ocean) from the perturbation approach agrees within 3% with the C_{ant} inventory in 2005 simulated by the more costly full biogeochemical approach (Terhaar et al., 2019). This relatively small difference between the two approaches probably results from most of the C_{ant} in the Arctic Ocean interior being taken up in the Atlantic Ocean or the Barents Sea, where the sea surface alkalinity is close to the perturbation approach's assumed 2,300µmol kg^{-1}. Thus, alkalinity and salinity anomalies at the Arctic Ocean surface due to freshwater input from rivers and

sea ice melt (Chierici & Fransson, 2009; Mathis et al., 2015; Semiletov et al., 2016) have little impact beyond its shallow surface waters. Because of limited computational resources, we used a coarser resolution version of the model (ORCA05, nominal resolution of 0.5°) from 1765 to 1957 and the higher resolution version (ORCA025, nominal resolution of 0.25°) only for the final 1958–2012 period. Also included in the model is CFC-12, an inert tracer that is simulated from 1932 onwards following the OCMIP-2 protocol (Dutay et al., 2002) but with the atmospheric boundary conditions from Bullister (2015).

2.3. TTD Calculation

The TTD approach was applied following Hall et al. (2002), Waugh et al. (2004), and Tanhua et al. (2009). The concentration of a tracer $c(r, t)$ was calculated at each point r and time t (in years) using the equation

$$c(r,t) = \int_0^\infty c_0(t-t')G_r(t')dt', \tag{6}$$

where $G_r(t')$ is the commonly applied inverse Gaussian of the Green's function (e.g., Olsen et al., 2010; Tanhua et al., 2009; Waugh et al., 2004; Waugh et al., 2006) and $c_0(t-t')$ is the tracer's surface-ocean time history with t being the year when the tracer concentration in the water cell is calculated and t' being the transit time of the water mass in years since it left the sea surface. The surface ocean time history of C_{ant} is calculated as the difference between C_T at time $t-t'$ and preindustrial C_T (year 1765), where C_T is calculated from the simulated temperature in the water cell, fixed salinity (35), and A_T (2,300μmol kg^{-1}), consistent with the perturbation simulation and the atmospheric pCO_2 in the respective year (Le Quéré et al., 2015; Meinshausen et al., 2017), assuming equilibrium between the atmosphere and the surface ocean. To calculate C_T from A_T and pCO_2, we used the MATLAB version of the routine CO2SYS (van Heuven et al., 2011) with K_1 and K_2 dissociation constants from Millero et al. (2002), the dissociation constant for boric acid from Dickson (1990), and the total boron-to-salinity ratio from Uppström (1974). The solubility of CO_2 was calculated following Weiss (1974). For these calculations, nutrient concentrations are assumed to be zero. Although phosphoric and silicic acid systems contribute to A_T and thus should be corrected for when calculating C_T, their effect is assumed to be negligible when calculating C_{ant}, a difference between C_T at time $t-t'$ and preindustrial C_T, both being biased similarly in the same direction.

For every water parcel r, $G_r(t')$ is expressed as

$$G_r(t') = \sqrt{\frac{\Gamma^3}{4\pi\Delta^2 t'^3}} exp\left(\frac{-\Gamma(t'-\Gamma)^2}{4\Delta^2 t'}\right), \tag{7}$$

where Δ represents the width of the TTD and Γ the mean age of the water parcel. The mean age was calculated at each point r, assuming $\Delta/\Gamma = 1$, from the measured CFC-12 concentration at time t ($c(r,t)$) and the surface ocean CFC-12 history ($c_0(t-t')$) calculated from the atmospheric history of the partial pressure of CFC-12 (pCFC-12) (Bullister, 2015), assuming equilibrium between pCFC-12 in the atmosphere and that in the surface ocean. The solubility of CFC-12 was calculated following Warner and Weiss (1985). Based on the mean age, $G_r(t')$ was derived at every point r.

In waters where pCFC-12 is supersaturated with respect to the current atmospheric pCFC-12, $G_r(t')$ cannot be derived; hence, the TTD method cannot be applied. Oceanic pCFC-12 can exceed atmospheric pCFC-12 because atmospheric CFC-12 levels have declined since 2002. Thus, when comparing C_{ant} calculated by the TTD method to that which is simulated directly, we masked out model grid cells where ocean pCFC-12 is above atmospheric pCFC-12, amounting to 6.5% of the total Arctic Ocean C_{ant} inventory in 2005 based on directly simulated C_{ant} (section 2.4). While the TTD method could not be evaluated in these supersaturated waters, they are included in data-based C_{ant} estimate from Tanhua et al. (2009) assuming a mean age of zero.

The ratio of Δ to Γ determines the relative importance of advection versus diffusion, with $\Delta/\Gamma < 1$ indicating a larger advective than diffusive share. Here, we used the typical Δ/Γ ratio of 1.0 (Tanhua et al., 2009; Waugh et al., 2006) as the standard case and assume the related $\pm 1\sigma$ uncertainty to be ±5% following Tanhua et al. (2008,2009). Furthermore, we made a series of sensitivity tests over a range of Δ/Γ ratios. When that ratio is varied between 0.6 and 1.8, vertical profiles of C_{ant}^{TTD} concentrations averaged over the Arctic Ocean still agree within the applied uncertainty of ±5% (Figure S1). In another study, Rajasakaren et al. (2019) compared mean ages derived from SF_6 with those derived from CFC-12 while varying the Δ/Γ ratio to identify the value of that ratio where the mean ages derived from both tracers agreed best. From their comparison, they provide a regionally varying best estimate of Δ/Γ for each Arctic Ocean water mass. Their estimates

range from 0.6 for Atlantic Water in the Amerasian basin to 1.2 for waters below the Atlantic Water layer. Their results also indicate that the C_{ant}^{TTD} concentration uncertainty related to the Δ/Γ ratio is at most ±5% (Rajasakaren et al., 2019, figures 8 and 11) in accord with our uncertainty estimation.

The TTD approach assumes that ocean circulation is in steady-state, that it can be represented by a 1-D advection-diffusion equation ($G_r(t')$), and that there is one surface-ocean source region for both tracers, C_{ant} and CFC-12. It also assumes that there is conservative mixing between water masses from different source regions and that the air-sea disequilibrium for both tracers is constant in time. In the standard case for TTD, it is assumed that there is no air-sea disequilibrium for either tracer.

2.4. Evaluation of TTD

To evaluate the TTD method, we applied it to simulated CFC-12 and temperature from the summer of 2005, that is, the year and months used for the TTD estimate from Tanhua et al. (2009). This TTD-based C_{ant} is denoted as C_{ant}^{TTD}. For consistency with the perturbation simulations, the A_T was fixed at 2,300 μmol kg^{-1}, the salinity at 35, and the atmospheric boundary conditions for CO_2 were identical. The TTD method was evaluated separately for SPW, WPW, AW, and BSW.

The TTD approach could not be evaluated in some parts of the Arctic Ocean because of our simulation strategy, which initialized all variables in the high-resolution configuration ORCA025 in 1958 with results from the coarse-resolution configuration ORCA05. Around 41% of the oceanic invasion of the directly simulated anthropogenic carbon (C_{ant}^{NEMO}) occurs before 1958 (with ORCA05), while only 2% of the oceanic CFC-12 invasion occurs before 1958 (with ORCA025) because of its more recent perturbation. While this 1958 initialization of ORCA025 with output of ORCA05 poses no problem for the evaluation of the TTD method in relatively young water masses, it biases the evaluation for older water masses where the circulation in ORCA05 differs largely from ORCA025. The largest differences between the two configurations is in the deep Arctic Ocean, where separate CFC-12 simulations indicate that waters are ventilated to 1,300-min ORCA05 and to 1,800-min ORCA025 (Terhaar et al., 2019). Thus, in the combined CFC-12 simulation (ORCA05 for 1932–1957, then ORCA025 for 1958–2012), simulated CFC-12 in year 2005 is relatively more abundant below 1,300 m, a signature of ORCA025, when compared to C_{ant}^{NEMO} (ORCA05 for 1765–1957, then ORCA025 for 1958–2012) in the same year because the anthropogenic carbon invasion began much earlier. That is, C_{ant}^{NEMO} depends more on the characteristics of the simulated circulation in ORCA05. Hence, in waters below 1,300 m, which represent 54% of the Arctic Ocean volume and 10% of the simulated Arctic Ocean C_{ant} inventory, it is inappropriate to evaluate the TTD method.

Furthermore, the evaluation should only be performed in regions where the model represents the Arctic Ocean circulation reasonably well. That is the case for most parts of the Arctic Ocean above 1,300 m except for the western end of the Canada basin, which receives no AW in the model (Terhaar et al., 2019). Consequently, the simulated CFC-12 concentrations remain close to zero and well below those observed (Tanhua et al., 2009). Hence, the TTD method is also not evaluated in that region, which represents 6% of Arctic Ocean volume and 10% of the simulated Arctic Ocean C_{ant} inventory. After excluding surface waters that were found to be supersaturated with respect to CFC-12 (3% of the Arctic Ocean's volume and 7% of its C_{ant} inventory), the TTD evaluation was performed in water masses representing 37% of the Arctic Ocean volume and 69% of the simulated Arctic Ocean C_{ant} inventory. Yet despite this partial coverage, results from the TTD evaluation were expanded upon by classifying each water parcel as a member of one of the Arctic's four dominant water masses and then applying the corresponding corrective factors.

2.5. Correction of C_{ant}

Each data-based C_{ant} concentration from Tanhua et al. (2009) was adjusted based on its assigned water mass, determined from its associated physical characteristics (Table S1), and the pertinent water-mass specific corrective factor from our evaluation of the TTD approach (section 3). Water masses between 250 and 800 m across the Arctic Ocean were mainly identified as AW (Smethie et al., 2000), while those below 800 m were largely identified as WPW (Aagaard, 1981; Swift et al., 1997) or BSW (Jones, 2001; Jones et al., 1995; Smedsrud et al., 2013).

2.6. Future C_{ant}

Coarse-resolution ocean models tend to underestimate the storage of C_{ant} in the Arctic Ocean and the resulting shoaling of the deep ASH (Terhaar et al., 2019). Yet 21st century projections with high-resolution

ocean-biogeochemical models remain prohibitive due to their computational costs. A simpler alternative is to estimate future C_{ant} concentrations based on the TTD approach.

Following Anderson et al. (2010), the TTD approach was used here to estimate C_{ant} concentrations along the Beringia 2005 section over the 21st century, but this time with atmospheric CO_2 from the four Representative Concentration Pathways RCP2.6, RCP4.5, RCP6.0, and RCP8.5 (Meinshausen et al., 2011) instead of with an exponentially increasing atmospheric CO_2. The TTD was estimated based on observed CFC-12, temperature, and salinity, while A_T was computed from salinity based on an Arctic-specific relationship (MacGilchrist et al., 2014). The computed TTD from observed CFC-12 in 2005 (equation 7) was then applied to atmospheric CO_2 levels for 13 different years spanning from 2014 to 2107 in each of the four RCP scenarios. The resulting ocean C_{ant} concentrations were then adjusted based on the corrective factors that were obtained from the TTD evaluation (section 3).

This TTD-based approach implicitly assumes no physical changes, for example, in ocean circulation, sea-ice extent, river discharge, temperature, salinity, and mixed-layer depth. It also assumes that the air-sea disequilibrium does not change with time. Furthermore, the TTD approach is based on tracers that started to invade the ocean more recently than anthropogenic carbon. To test if the accuracy of the TTD method changes when being applied to a tracer with a longer atmospheric history, we replicated our TTD-based future estimates and compared them to model estimates using the computationally efficient, coarse-resolution version of the model (ORCA2, nominal horizontal resolution of 2°). In ORCA2, we simulated CFC-12 over 1932–2005 and C_{ant} over 1765–2100. The simulated CFC-12 concentrations in 2005 were used to derive the TTD. This TTD was then combined with atmospheric CO_2 levels over 1765–2005 and over 1765–2100 to estimate C_{ant} concentrations in the ocean. Despite the considerably longer atmospheric history of C_{ant} in 2100, the relative uncertainty of the TTD estimated C_{ant} concentrations remains almost the same (Figure S2). Although ORCA2 does not simulate the Arctic Ocean circulation as well as ORCA025 (Terhaar et al., 2019), the relative uncertainty of its C_{ant}^{TTD} concentrations in 2005 remains similar to that in 2100 over the range of observed CFC-12 concentrations and thus over the range of observed mean ages. Thus, it appears that the TTD computed from present-day CFC-12 may be used to estimate C_{ant} uptake over 1765–2100 for the idealized case where atmospheric CO_2 increases but climate and the air-sea disequilibrium do not change.

2.7. Ω_A and Undersaturation Index

The aragonite saturation state Ω_A was calculated using mocsy (Orr & Epitalon, 2015) with dissociation constants recommended for best practices (Dickson et al., 2007). Combined standard uncertainties in Ω_A were computed from the standard uncertainties in the dissociation constants and the solubility product for aragonite (Mucci, 1983) using mocsy's uncertainty propagation routine from Orr et al. (2018). Due to the idealized nature of our simulated future estimates, we neglected measurement uncertainties for the CO_2 system input variables (A_T and C_T).

Present-day Ω_A was calculated from observed temperature, salinity, C_T, A_T, total dissolved inorganic phosphorus (P_T), total dissolved silicon (Si_T), and depth along the Beringia 2005 section. Preindustrial Ω_A was computed after subtracting the adjusted C_{ant} concentration estimates in 2005 from measured C_T and assuming that the other variables did not change over the industrial period. For estimates of Ω_A over the 21st century, the changes in the C_{ant} concentrations since 2005 were added to C_T measurements taken in 2005, while also neglecting changes in all other variables.

The basin-wide undersaturation with respect to aragonite was characterized by the undersaturation index (UI), the fraction of the total Arctic Ocean volume where $\Omega_A < 1$. Here, UI is based on Ω_A at the measurement points along the Beringia section, weighted by depth and distance. It is not extrapolated beyond the Beringia section to other parts of the Arctic basin.

3. Evaluation of TTD Method in the Arctic Ocean

In the Arctic Ocean, the ORCA025 configuration of NEMO-PISCES, which is initialized in 1958 with output from the ORCA05 configuration, simulates a total C_{ant}^{NEMO} inventory of 2.5 Pg C in 2005. That simulated inventory lies at the lower end of the uncertainty range of the data-based estimate from Tanhua et al. (2009) (2.5–3.3 Pg C in 2005) because of (1) the model's inadequate horizontal extension of Atlantic Waters at intermediate depths and (2) its insufficient deep-water formation (Terhaar et al., 2019). After masking out cells where the *p*CFC-12 level in the ocean exceeds that in the atmosphere, owing to the decline in atmospheric

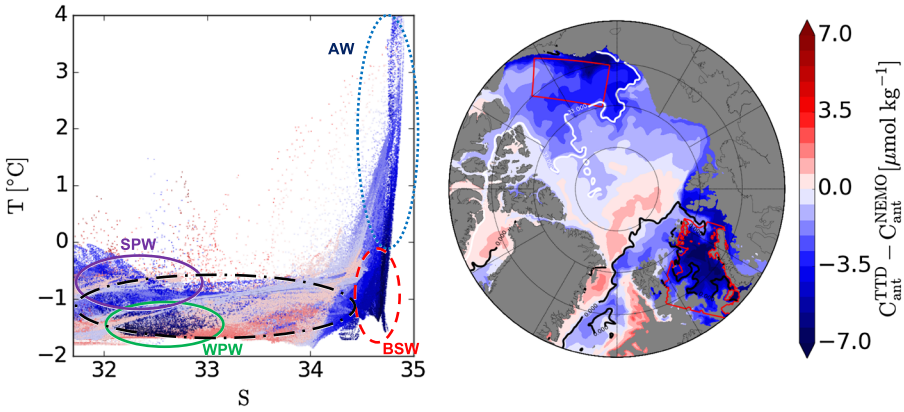

Figure 1. Gas saturation of simulated surface-ocean δpCO_2 and *p*CFC-12 relative to atmospheric values during the seasonal cycle in 2005 shown as averages for the Barents Sea and the Chukchi Sea (regions indicated in Figure 2). The dotted horizontal line indicates air-sea equilibrium. The shaded blue area indicates the period of deep-water formation, defined as the period with the lowest density gradient between surface ocean and the deep waters in the Barents Sea and Chukchi Sea. The red arrow indicates the difference in saturation between δpCO_2 and simulated *p*CFC-12.

CFC-12 concentrations since 2002, the C_{ant}^{NEMO} inventory is reduced to 2.3 Pg C. In comparison, the C_{ant}^{TTD} inventory (calculated from simulated CFC-12, T, and S) in the Arctic Ocean is 2.2 Pg C.

The difference between C_{ant}^{TTD} and C_{ant}^{NEMO} would be expected to be larger had we used ORCA025 before 1958 instead of the coarser configuration ORCA05, which simulates less storage of C_{ant} (Terhaar et al., 2019). Indeed, when evaluating the TTD approach in the model's younger waters that are affected little by the change in resolution in 1958, the calculated C_{ant}^{TTD} concentrations are seen to underestimate the reference C_{ant}^{NEMO} concentrations by $7 \pm 2\%$ (2.5 ± 0.9 μmol kg^{-1}) in SPW, by $12 \pm 3\%$ (4.9 ± 1.3 μmol kg^{-1}) in WPW, by $4 \pm 2\%$ (1.1 ± 0.6 μmol kg^{-1}) in AW, and by $12 \pm 2\%$ (5.0 ± 1.1 μmol kg^{-1}) in BSW (Table S1).

The general underestimation of C_{ant} by the TTD method can be explained by its simplified assumption for the saturation of surface ocean δpCO_2 and *p*CFC-12 relative to the atmosphere during deep-water formation in the Arctic Ocean (Figure 1). Contrary to the TTD assumption of perfect equilibrium between the atmosphere and the surface ocean for both δpCO_2 and *p*CFC-12, during deep-water formation in February and March, simulated δpCO_2 in the surface ocean is higher than atmospheric δpCO_2; it is supersaturated. Conversely, surface ocean *p*CFC-12 is lower than atmospheric *p*CFC-12; it is undersaturated. This disequilibrium between the surface ocean and atmosphere for both δpCO_2 and *p*CFC-12 can be attributed to the rapid heat loss of inflowing PW and AW (Kaltin & Anderson, 2005; Midttun, 1985). For any gas (e.g., CFC-12), when surface cooling is faster than its air-sea equilibration, then the dissolved gas concentration changes little and its partial pressure must decline (e.g., see Orr et al., 2017, eq. 21). Conversely, δpCO_2 (the anthropogenic change in pCO_2) depends on ocean chemistry. Cooling causes oceanic δpCO_2 to increase because it reduces the carbonate ion concentration and thus the buffer capacity, making the water less able to retain anthropogenic carbon.

Air-sea equilibration also depends on how long waters remain at the surface and the extent to which those surface waters are ice free. Surface-water transit times in the Barents and Chukchi Seas are around 6 months each (Loeng, 1991; Spall, 2007). During that transit, the surface waters undergo continual cooling in the Barents Sea and are isolated by substantial sea-ice cover in the Chukchi Sea. Hence, gas equilibrium between air and sea is not reached, neither for δpCO_2 nor for *p*CFC-12, before those surface waters are subducted. Thus, the TTD assumption that both δpCO_2 and *p*CFC-12 in those surface waters equilibrate entirely with the atmosphere causes the TTD-based estimates of C_{ant} concentrations to be too low in the deep waters that were formed from surface waters in the Chukchi and Barents Seas.

The TTD approach's largest underestimates are found in WPW in the Chukchi Sea, delimited by the S = 33 contour in Figure 2, and in the BSW, delimited by the 0°C isotherm in the same figure. The extent of underestimation diminishes as these water masses mix with others (Figure 2). The bias in the BSW is reduced once it enters the Nansen basin and mixes with AW. A signature of this mixing in the model is its decrease in the

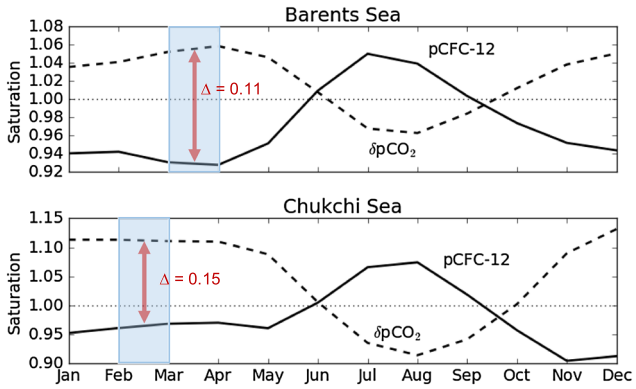

Figure 2. Difference between anthropogenic carbon concentrations C_{ant}^{NEMO} that are simulated directly (C_{ant}^{NEMO}) and those that are estimated indirectly by applying the TTD approach in the model (C_{ant}^{TTD}). Differences are shown for all grid cells in the top 160 m as a function of simulated temperature and salinity (left) and on a map at 112 m, below the stratified surface waters (right). Colored ellipses indicate BSW (red dashed), AW (blue dotted), SPW (magenta solid), WPW (green solid), and the remaining waters close to the surface (black dash-dotted). The regions in the Chukchi Sea and the Barents Seat that are outlined in red on the map are those for which averages are shown in Figure 1.

temperature gradient in the AW along the shelf-break of the Nansen basin, a feature that is also observed (Gammelsrød et al., 2009; Schauer et al., 2002).

4. Correction of Data-Based Estimate of C_{ant}

To refine the data-based estimate from Tanhua et al. (2009), we adjusted their TTD-based estimates upward based on the extent of underestimation in each water mass indicated by our model-based assessment. That is, we assigned corrective factors for the C_{ant} concentrations to each water mass: +4% for AW, +12% for WPW and BSW, and +7% for SPW (section 3, Table S1). After this adjustment of the TTD-based C_{ant} concentrations, the best estimate for the Arctic Ocean C_{ant} inventory increases from 3.0 to 3.3 Pg C in 2005 while the uncertainty range changes from 2.5–3.3 to 3.0–3.6 Pg C. The lower bound of the uncertainty range increases by 0.2 Pg C more than the upper bound, reducing the overall uncertainty range. The former lower bound accounted for the additional uncertainty for the bias between surface saturations of δpCO_2 and pCFC-12 (Tanhua et al., 2009), an estimate that was based on results from the Southern Ocean (Waugh et al., 2006). Here, we explicitly account for the sign and magnitude of these saturation differences in the Arctic.

The remaining uncertainty of the C_{ant} inventory is considered the same as previously estimated by Tanhua et al. (2008, 2009). It includes uncertainties from the Δ/Γ ratio (±5%), from the spatial extrapolation (±5%), and from either very low CFC-12 concentrations in old waters or supersaturation of CFC-12 in young waters owing to the decline in atmospheric CFC-12 since 2002 (±7%). Rajasakaren et al. (2019) also estimated uncertainties from the Δ/Γ ratio and from their lateral extrapolation of C_{ant}^{TTD} concentrations from the Beringia section to the entire Arctic Ocean. While their uncertainty from the Δ/Γ ratio is also around ±5% (Rajasakaren et al., 2019, figures 8 and 11), they estimate a 50% uncertainty from their spatial extrapolation. Conversely, Tanhua et al. (2009) estimate only a 5% extrapolation uncertainty, an estimate we adopt here. While Rajasakaren et al. (2019) rely on tracer measurements along only the Beringia section in 2005 (23 stations), Tanhua et al. (2009) exploited many more tracer measurements during 1983 to 2005 (535 stations), scaling those to 2005. Although Tanhua et al.'s temporal scaling adds some uncertainty, their use of much more data covering most parts of the four major basins dramatically reduces the overall uncertainty.

5. Arctic Ocean Acidification

Using the data-based C_{ant}^{obs} concentration estimates from Tanhua et al. (2009), Anderson et al. (2010) calculated that the average depth of the ASH on the Beringia section was 1,890 m in 2005 and that it had shoaled by 190 m between 1765 and 2005. Based on our refined C_{ant} concentration estimates, the distance-weighted mean ASH along that section is located at 1,950 ± 260 m in 2005 and it has shoaled by 270 ± 60 m during 1765–2005, that is, by 37% more on average than estimated by Anderson et al. (2010). Error bars represent plus or minus one combined standard uncertainty from the propagation of the standard uncertainties of the dissociation constants and the solubility product for aragonite.

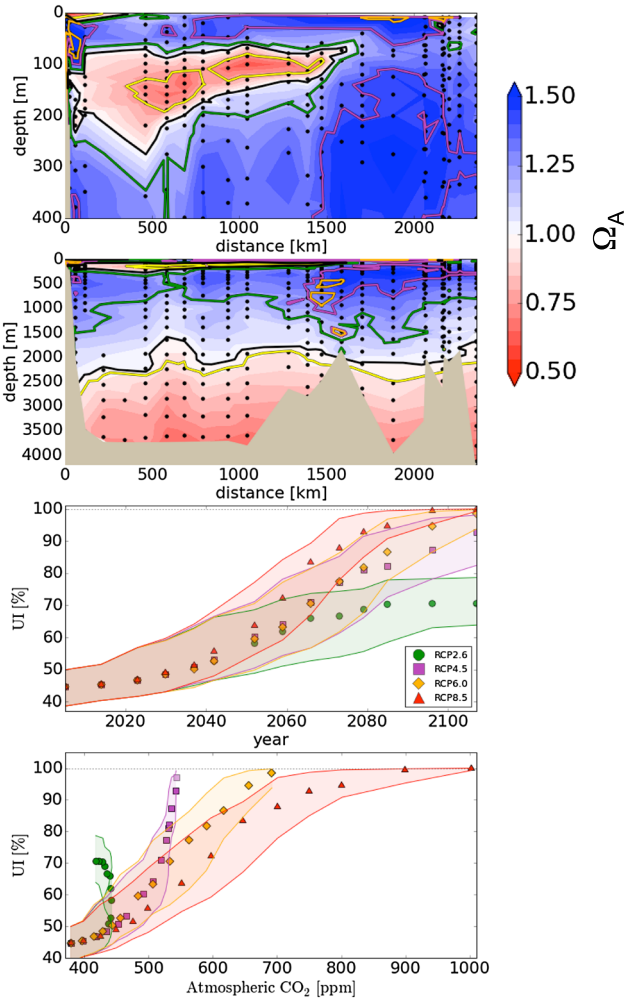

Figure 3. The Ω_A and ASH along the Beringia 2005 section over the upper 400 m(top) and over the full water column (upper middle) along with estimates of the time evolution of UI based on four RCP scenarios displayed as a function of year (lower middle) and of atmospheric CO_2 (bottom). In the top two panels, shading indicates the observed 2005 conditions. Also shown is the ASH for 2005 (black), for the preindustrial back calculation (yellow), and for 2107 for three future scenarios: RCP2.6 (green), RCP4.5 (magenta), and RCP6.0 (orange). Shaded areas in the bottom two panels indicate the combined standard uncertainties propagated from standard uncertainties in the carbonate system dissociation constants and the solubility product for aragonite. The lighter purple marker in the bottom panel is for RCP4.5 in year 2150.

Furthermore, we assessed the spatial variability of the depth of the ASH along the Beringia section. In 2005, that section's deepest ASH (2,450 ± 300m) is found on the continental rise next to the Beaufort Sea, while its shallowest ASH (1,590 ± 300 m) is 500 km away in the center of the Canada basin (Figure 3). Shoaling also varies along the section, from as low as 80 m in the southern part of the Canada basin to as much as 550 m in the center of the Canada basin.

For the future scenarios, we applied the same basic approach as used by Anderson et al. (2010), which considers that changes in Ω_A are only due to the direct effect of increasing atmospheric CO_2 on ocean chemistry; effects from climate change are ignored. Thus, we applied the observation-based TTD obtained for 2005 along the Beringia section to the four future RCP scenarios to estimate the evolution of C_{ant} concentrations and UI along the same section as described in section 2.7 (Figure 3). Between 2005 to 2037, the UI follows the same trajectory under all four RCPs, increasing from 39–50% to 45–64%. Afterwards, it diverges. Under RCP2.6, the UI rises more slowly reaching 63–78% in 2087 and remains constant thereafter. Under the three other RCP scenarios, the UI increases more quickly, for example, in 2100 reaching 80–97% under RCP4.5, 90–100% under RCP6.0, and 97–100% under RCP8.5.

Our idealized TTD-based estimates were also compared to simulated changes in Ω_A from Steinacher et al. (2009), who made projections with the NCAR CSM1.4 climate-carbon model. During the 21st century, their model is forced under the Special Report on Emissions Scenarios (SRES) B1 and A2, which are similar to the more recent RCP2.6 and RCP8.5 scenarios used here. Steinacher et al. found that in 2100, the entire water column in the Arctic Ocean becomes undersaturated with respect to aragonite under the A2 scenario but not under the B1 scenario. That complete undersaturation under the A2 scenario occurs in 2090 when atmospheric CO_2 reaches 765 ppm. Likewise, our results suggest that the Arctic water column would become entirely undersaturated by 2100 (Figure 3) under the RCP8.5 scenario, when atmospheric CO_2 reaches 936 ppm, but not under the lower atmospheric CO_2 levels of the RCP2.6 scenario, which reaches 443 ppm in 2052 and subsequently declines. Our results also suggest that the Arctic Ocean would eventually become almost entirely undersaturated (UI > 95%) even at atmospheric CO_2 levels less than 765 ppm.

With the two intermediate RCP scenarios, the UI reaches 93–99% in 2150 under RCP4.5 and 94–100% under RCP6.0. The lowest atmospheric CO_2 level at which nearly complete undersaturation (UI > 95%) is reached is 540 ppm, the atmospheric CO_2 value at which RCP4.5 levels out. Under the RCP8.5 scenario, the 540 ppm threshold is reached sooner, in 2051, but the entire Arctic water column does not become undersaturated until 2080 because it takes time to ventilate intermediate and deep waters. These findings emphasize that the year in which the entire Arctic Ocean water column would become undersaturated with respect to aragonite depends not only on reaching a specific atmospheric CO_2 level but also on the rates of increase and future decline. Complete undersaturation of the Arctic Ocean appears inevitable if atmospheric CO_2 would reach twice the preindustrial level unless just afterwards there were a sharp decline.

Unlike model studies (Steinacher et al., 2009; Steiner et al., 2013), our future estimates are based on data-based estimates of the ventilation age and future RCP scenarios of atmospheric CO_2. This simplified approach suggests that during the 21st century under RCP8.5, the deep ASH would shoal by 900 m, nine times as much as found with the model studies. In contrast, the model studies suggest much greater deepening of undersaturated waters from the surface before there is a merge with the models' more

slowly shoaling deep ASH, at which time the entire water column becomes undersaturated. However, these coarse-resolution ocean models largely underestimate lateral input of C_{ant} into the Arctic Ocean (Terhaar et al., 2019). Their resulting underestimated storage of C_{ant} in intermediate waters implies that they also underestimate the shoaling of the deep ASH.

Our TTD-based estimates of increasing C_{ant} concentrations and resulting acidification during the 21st century account for future invasion of C_{ant} but neglect climate change and its affect on the ocean. Yet the Arctic Ocean is already experiencing changes in sea-ice extent (Serreze & Stroeve, 2015) and primary production (Arrigo & van Dijken, 2015). During this century, the Arctic Ocean is also projected to experience large increases in summertime sea-surface temperature (Carton et al., 2015). All of these changes will affect Arctic Ocean uptake of C_{ant} and hence its acidification. Steinacher et al. (2009) estimate with their model projection that the dominant climate-change effect on Ω_A is a reduction due to dilution of C_T and A_T from sea-ice melt. Climate change is also expected to alter the Arctic Ocean circulation and the associated transport of C_{ant} into the deep Arctic Ocean, although the primary driver of overall change in Ω_A is the increase in C_{ant}. Lique et al. (2018) found that the climate-change-induced brine rejection from sea-ice melt intensified deep-water convection in the Eurasian basin in the HiGEM climate model forced under a $4\times CO_2$ scenario. Some indication for this projected increase in deep-water formation in the Arctic Ocean appears to have already been observed, namely, through an increased contribution of Arctic waters to deep water masses in the Nordic Seas (Langehaug & Falck, 2012; Somavilla et al., 2013). More Arctic deep convection would further enhance Arctic storage of C_{ant} and thus deep-water acidification and shoaling of the deep ASH. Steinacher et al. (2009) found that the effects of climate change will enhance the reduction of Ω_A in the Arctic Ocean. Thus, our estimate of the future reduction in Arctic Ocean Ω_A, which neglects climate change, should be considered as a lower bound. Despite the uncertainties associated with the idealized nature of our study, including its neglect of climate change and observational uncertainties, it is consistent with previous studies in estimating that in coming years the Arctic Ocean will experience widespread undersaturation with respect to aragonite, a dramatic chemical change that is expected to degrade the Arctic Ocean ecosystem (Fabry et al., 2008; Gattuso & Hansson, 2011; Riebesell et al., 2013).

6. Conclusion

Our model-based evaluation has demonstrated that the TTD approach underestimates C_{ant} concentrations in the Arctic Ocean by up to 12% depending on the water mass considered. These underestimates occur throughout the water column, being tied through water-mass formation to biases in surface waters. The surface C_{ant} concentrations estimated by TTD are generally too low because of that approach's assumption of perfect gas equilibrium between the surface ocean and the atmosphere for both δpCO_2 and pCFC-12. In contrast, our ocean model produces surface-ocean δpCO_2 that is supersaturated with respect to atmospheric δpCO_2 at the time of deep-water formation, while also producing surface ocean pCFC-12 that is undersaturated relative to atmospheric pCFC-12. Not accounting for these contrasting tendencies biases the TTD approach. After adjusting the 2005 Arctic Ocean C_{ant} inventory from Tanhua et al. (2009) for these biases, the best estimate of that inventory increases from 3.0 to 3.3 Pg C while the uncertainty range moves from 2.5–3.3 to 3.0–3.6 Pg C.

By using the bias-corrected TTD approach with future atmospheric CO_2 scenarios, we provide an estimate of future conditions for an idealized case where effects from climate change are neglected. Results from that simplified analysis suggest that the Arctic Ocean would eventually become entirely undersaturated with respect to aragonite unless atmospheric CO_2 were stabilized below 540 ppm. Avoiding an entirely undersaturated Arctic Ocean would thus not be possible under the RCP4.5 scenario, which maintains that CO_2 level after 2100. Effects from climate change would probably reduce that atmospheric CO_2 threshold. Retaining some Arctic Ocean waters that are not corrosive to aragonite appears feasible only under more optimistic scenarios such as RCP2.6. To better characterize the atmospheric CO_2 stabilization threshold at which the Arctic Ocean would eventually become entirely undersaturated with respect to aragonite, more studies are needed with Earth System Models forced under stabilization scenarios beyond 2100.

Data Availability Statement

Model output was analyzed on CICLAD at IPSL and is openly accessible on the ODATIS-supported center SEANOE (https://www.seanoe.org/data/00628/74022/).

Acknowledgments
This study was funded through the EU H2020 project C-CASCADES (Marie Sklodowska-Curie Grant 643052). Support for coauthors is acknowledged from the French Agence Nationale de la Recherche (ANR) project SOBUMS (ANR-16-CE01-0014), the MTES/FRB Acidoscope project, and the EU H2020 projects CRESCENDO (Grant 641816), VERIFY (Grant 776810), and COMFORT (Grant 820989). Simulations were performed using HPC resources from GENCI-TGCC and GENCI-IDRIS (Grant 2018-A0050100040).

References

Aagaard, K. (1981). On the deep circulation in the Arctic Ocean. *Deep-Sea Research Part I*, *28*(3), 251–268. https://doi.org/10.1016/0198-0149(81)90066-2

Anderson, L., Tanhua, T., Björk, G., Hjalmarsson, S., Jones, E., Jutterström, S., et al. (2010). Arctic Ocean shelf-basin interaction: An active continental shelf CO_2 pump and its impact on the degree of calcium carbonate solubility. *Deep-Sea Research Part I*, *57*(7), 869–879. https://doi.org/10.1016/j.dsr.2010.03.012

Arrigo, K. R., & van Dijken, G. L. (2015). Continued increases in Arctic Ocean primary production. *Progress in Oceanography*, *136*, 60–70. https://doi.org/10.1016/j.pocean.2015.05.002

Atamanchuk, D., Koelling, J., Send, U., & Wallace, D. (2020). Rapid transfer of oxygen to the deep ocean mediated by bubbles. *Nature Geoscience*, *13*(3), 232–237. https://doi.org/10.1038/s41561-020-0532-2

Bates, N. R., & Mathis, J. T. (2009). The Arctic Ocean marine carbon cycle: Evaluation of air-sea CO_2 exchanges, ocean acidification impacts and potential feedbacks. *Biogeosciences*, *6*(11), 2433–2459. https://doi.org/10.5194/bg-6-2433-2009

Bourgain, P., Gascard, J. C., Shi, J., & Zhao, J. (2013). Large-scale temperature and salinity changes in the upper canadian basin of the Arctic Ocean at a time of a drastic Arctic Oscillation inversion. *Ocean Science*, *9*(2), 447–460. https://doi.org/10.3402/tellusa.v26i1-2.9733

Broecker, W. S., & Peng, T.-H. (1974). Gas exchange rates between air and sea. *Tellus*, *26*, 21–35. https://doi.org/10.1111/j.2153-3490.1974.tb01948.x

Bullister, J. L. (2015). *Atmospheric Histories (1765-2015) for CFC-11, CFC-12, CFC-113, CCl_4, SF_6 and N_2O, Carbon Dioxide Information Analysis Center, Oak Ridge National Laboratory US Department of Energy, ORNL/CDIAC-161, NDP-095*, https://doi.org/10.3334/CDIAC/otg.CFC_ATM_Hist_2015. Tennessee: Oak Ridge. http://cdiac.ornl.gov/ftp/oceans/CFC_ATM_Hist/CFC_ATM_Hist_2015

Carton, J. A., Ding, Y., & Arrigo, K. R. (2015). The seasonal cycle of the Arctic Ocean under climate change. *Geophysical Research Letters*, *42*, 7681–7686. https://doi.org/10.1002/2015GL064514

Chierici, M., & Fransson, A. (2009). Calcium carbonate saturation in the surface water of the Arctic Ocean: undersaturation in freshwater influenced shelves. *Biogeosciences*, *6*(11), 2421–2431. https://doi.org/10.5194/bg-6-2421-2009

Dickson, A. G. (1990). Standard potential of the reaction: $AgCl(s) + 12h_2(g) = Ag(s) + HCl(aq)$, and the standard acidity constant of the ion HSO_4^- in synthetic sea water from 273.15 to 318.15 k. *The Journal of Chemical Thermodynamics*, *22*(2), 113–127. https://doi.org/10.1016/0021-9614(90)90074-Z

Dickson, A. G., Sabine, C. L., & Christian, J. R. (2007). Guide to best practices for ocean CO_2 measurements, tech. rep.: PICES Special Publication.

Dutay, J.-C., Bullister, J., Doney, S., Orr, J., Najjar, R., Caldeira, K., et al. (2002). Evaluation of ocean model ventilation with CFC-11: comparison of 13 global ocean models. *Ocean Modelling*, *4*(2), 89–120. https://doi.org/10.1016/S1463-5003(01)00013-0

Fabry, V. J., Seibel, B. A., Feely, R. A., & Orr, J. C. (2008). Impacts of ocean acidification on marine fauna and ecosystem processes, ICES. *Journal of Marine Science*, *65*(3), 414–432. https://doi.org/10.1093/icesjms/fsn048

Gammelsrød, T., Leikvin, Ø., Lien, V., Budgell, W. P., Loeng, H., & Maslowski, W. (2009). Mass and heat transports in the NE Barents Sea: Observations and models. *Journal of Marine Systems*, *75*(1), 56–69. https://doi.org/10.1016/j.jmarsys.2008.07.010

Gattuso, J.-P., & Hansson, L. (2011). *Ocean acidification*. Oxford: Oxford University Press.

Hall, T. M., Haine, T. W., & Waugh, D. W. (2002). Inferring the concentration of anthropogenic carbon in the ocean from tracers. *Global Biogeochemical Cycles*, *16*(4), 1131. https://doi.org/10.1029/2001GB001835

Hamme, R. C., Emerson, S. R., Severinghaus, J. P., Long, M. C., & Yashayaev, I. (2017). Using noble gas measurements to derive air-sea process information and predict physical gas saturations. *Geophysical Research Letters*, *44*, 9901–9909. https://doi.org/10.1002/2017GL075123

Jones, E. P. (2001). Circulation in the Arctic Ocean. *Polar Research*, *20*(2), 139–146. https://doi.org/10.1111/j.1751-8369.2001.tb00049.x

Jones, E., Rudels, B., & Anderson, L. (1995). Deep waters of the Arctic Ocean: Origins and circulation. *Deep-Sea Research Part I*, *42*(5), 737–760. https://doi.org/10.1016/0967-0637(95)00013-V

Kaltin, S., & Anderson, L. G. (2005). Uptake of atmospheric carbon dioxide in Arctic shelf seas: evaluation of the relative importance of processes that influence pCO_2 in water transported over the Bering-Chukchi Sea shelf. *Marine Chemistry*, *94*(1), 67–79. https://doi.org/10.1016/j.marchem.2004.07.010

Khatiwala, S., Tanhua, T., Fletcher, S. M., Gerber, M., Doney, S., Graven, H., et al. (2013). Global ocean storage of anthropogenic carbon. *Biogeosciences*, *10*(4), 2169–2191. https://doi.org/10.5194/bg-10-2169-2013

Lachkar, Z., Orr, J. C., Dutay, J.-C., & Delecluse, P. (2007). Effects of mesoscale eddies on global ocean distributions of CFC-11, CO_2, and $\Delta^{14}C$. *Ocean Science*, *3*(4), 461–482. https://doi.org/10.5194/os-3-461-2007

Langehaug, H. R., & Falck, E. (2012). Changes in the properties and distribution of the intermediate and deep waters in the Fram Strait. *Progress in Oceanography*, *96*(1), 57–76. https://doi.org/10.1016/j.pocean.2011.10.002

Le Quéré, C., Moriarty, R., Andrew, R., Peters, G., Ciais, P., Friedlingstein, P., et al. (2015). Global carbon budget 2014. *Earth System Science Data*, *7*(1), 47–85. https://doi.org/10.5194/essd-7-47-2015

Lique, C., Johnson, H. L., & Plancherel, Y. (2018). Emergence of deep convection in the Arctic Ocean under a warming climate. *Climate Dynamics*, *50*(9), 3833–3847. https://doi.org/10.1007/s00382-017-3849-9

Loeng, H. (1991). Features of the physical oceanographic conditions of the Barents Sea. *Polar Research*, *10*(1), 5–18. https://doi.org/10.3402/polar.v10i1.6723

Lueker, T. J., Dickson, A. G., & Keeling, C. D. (2000). Ocean pCO_2 calculated from dissolved inorganic carbon, alkalinity, and equations for K1 and K2: Validation based on laboratory measurements of CO_2 in gas and seawater at equilibrium. *Marine Chemistry*, *70*(1), 105–119. https://doi.org/10.1016/S0304-4203(00)00022-0

MacGilchrist, G., Garabato, A. N., Tsubouchi, T., Bacon, S., Torres-Valdes, S., & Azetsu-Scott, K. (2014). The Arctic Ocean carbon sink. *Deep Sea Research Part 1*, *86*, 39–55. https://doi.org/10.1016/j.dsr.2014.01.002

Madec, G. (2008). NEMO ocean engine, Note du Pôle de modélisation, Institut Pierre-Simon Laplace (IPSL), France.

Matear, R. J., Wong, C. S., & Xie, L. (2003). Can CFCs be used to determine anthropogenic CO_2? *Global Biogeochemical Cycles*, *17*(1), 1013. https://doi.org/10.1029/2001GB001415

Mathis, J. T., Cross, J. N., Evans, W., & Doney, S. C. (2015). Ocean acidification in the surface waters of the Pacific-Arctic boundary regions. *Oceanography*, *28*(2), 122–135. https://doi.org/10.5670/oceanog.2015.36

Matsumoto, K., & Gruber, N. (2005). How accurate is the estimation of anthropogenic carbon in the ocean? An evaluation of the ΔC^* method. *Global Biogeochemical Cycles*, *19*, GB3014. https://doi.org/10.1029/2004gb002397

Meinshausen, M., Smith, S. J., Calvin, K., Daniel, J. S., Kainuma, M. L. T., Lamarque, J.-F., et al. (2011). The RCP greenhouse gas concentrations and their extensions from 1765 to 2300. *Climate Change*, *109*(1), 213. https://doi.org/10.1007/s10584-011-0156-z

Meinshausen, M., Vogel, E., Nauels, A., Lorbacher, K., Meinshausen, N., Etheridge, D. M., et al. (2017). Historical greenhouse gas concentrations for climate modelling (CMIP6). *Geoscientific Model Development*, *10*(5), 2057–2116. https://doi.org/10.5194/gmd-10-2057-2017

Midttun, L. (1985). Formation of dense bottom water in the Barents Sea. *Deep Sea Research Part A*, *32*(10), 1233–1241. https://doi.org/10.1016/0198-0149(85)90006-8

Millero, F. J., Pierrot, D., Lee, K., Wanninkhof, R., Feely, R., Sabine, C. L., et al. (2002). Dissociation constants for carbonic acid determined from field measurements. *Deep-Sea Research Part I*, *49*(10), 1705–1723. https://doi.org/10.1016/S0967-0637(02)00093-6

Mucci, A. (1983). The solubility of calcite and aragonite in seawater at various salinities, temperatures, and one atmosphere total pressure. *American Journal of Science*, *283*, 780–799. https://doi.org/10.2475/ajs.283.7.780

Olsen, A., Omar, A. M., Jeansson, E., Anderson, L. G., & Bellerby, R. G. J. (2010). Nordic seas transit time distributions and anthropogenic CO_2. *Journal of Geophysical Research*, *115*, C05005. https://doi.org/10.1029/2009JC005488

Orr, J. C., & Epitalon, J.-M. (2015). Improved routines to model the ocean carbonate system: mocsy 2.0. *Geoscientific Model Development*, *8*(3), 485–499. https://doi.org/10.5194/gmd-8-485-2015, .

Orr, J. C., Epitalon, J.-M., Dickson, A. G., & Gattuso, J.-P. (2018). Routine uncertainty propagation for the marine carbon dioxide system. *Marine Chemistry*, *207*, 84–107. https://doi.org/10.1016/j.marchem.2018.10.006

Orr, J. C., Fabry, V. J., Aumont, O., Bopp, L., Doney, S. C., Feely, R. A., et al. (2005). Anthropogenic ocean acidification over the twenty-first century and its impact on calcifying organisms. *Nature*, *437*(7059), 681–686. https://doi.org/10.1038/nature04095

Orr, J. C., Najjar, R. G., Aumont, O., Bopp, L., Bullister, J. L., Danabasoglu, G., et al. (2017). Biogeochemical protocols and diagnostics for the CMIP6 ocean model intercomparison project (OMIP). *Geoscientific Model Development*, *10*(6), 2169–2199. https://doi.org/10.5194/gmd-10-2169-2017

Palmiéri, J., Orr, J., Dutay, J.-C., Béranger, K., Schneider, A., Beuvier, J., & Somot, S. (2015). Simulated anthropogenic CO_2 storage and acidification of the Mediterranean Sea. *Biogeosciences*, *12*(3), 781–802. https://doi.org/10.5194/bg-12-781-2015

Pickart, R. S., Weingartner, T. J., Pratt, L. J., Zimmermann, S., & Torres, D. J. (2005). Flow of winter-transformed Pacific water into the Western Arctic. *Deep Sea Research Part II*, *52*(24), 3175–3198. https://doi.org/10.1016/j.dsr2.2005.10.009

Rajasakaren, B., Jeansson, E., Olsen, A., Tanhua, T., Johannessen, T., & Smethie, W. (2019). Trends in anthropogenic carbon in the Arctic Ocean. *Progress in Oceanography*, *178*(102), 177. https://doi.org/10.1016/j.pocean.2019.102177

Riebesell, U., Gattuso, J.-P., Thingstad, T. F., & Middelburg, J. J. (2013). Arctic Ocean acidification: pelagic ecosystem and biogeochemical responses during a mesocosm study. *Biogeosciences*, *10*(8), 5619–5626. https://doi.org/10.5194/bg-10-5619-2013

Sarmiento, J. L., Orr, J. C., & Siegenthaler, U. (1992). A perturbation simulation of CO_2 uptake in an ocean general circulation model. *Journal of Geophysical Research*, *97*(C3), 3621–3645. https://doi.org/10.1029/91JC02849

Schauer, U., Loeng, H., Rudels, B., Ozhigin, V. K., & Dieck, W. (2002). Atlantic Water flow through the Barents and Kara Seas. *Deep-Sea Research Part I*, *49*(12), 2281–2298. https://doi.org/10.1016/S0967-0637(02)00125-5

Semiletov, I., Pipko, I., Gustafsson, Ö., Anderson, L. G., Sergienko, V., Pugach, S., et al. (2016). Acidification of East Siberian Arctic Shelf waters through addition of freshwater and terrestrial carbon. *Nature Geoscience*, *9*(5), 361–365. https://doi.org/10.1038/ngeo2695

Serreze, M. C., & Stroeve, J. (2015). Arctic sea ice trends, variability and implications for seasonal ice forecasting. *Philosophical Transactions of the Royal Society A*, *373*, 2045. https://doi.org/10.1098/rsta.2014.0159

Smedsrud, L. H., Esau, I., Ingvaldsen, R. B., Eldevik, T., Haugan, P. M., Li, C., et al. (2013). The role of the Barents Sea in the Arctic climate system. *Reviews of Geophysics*, *51*, 415–449. https://doi.org/10.1002/rog.20017

Smethie, W. M., Schlosser, P., BöNisch, G., & Hopkins, T. S. (2000). Renewal and circulation of intermediate waters in the Canadian Basin observed on the SCICEX 96 cruise. *Journal of Geophysical Research: Oceans*, *105*(C1), 1105–1121. https://doi.org/10.1029/1999JC900233

Somavilla, R., Schauer, U., & Budéus, G. (2013). Increasing amount of Arctic Ocean deep waters in the Greenland Sea. *Geophysical Research Letters*, *40*, 4361–4366. https://doi.org/10.1002/grl.50775

Spall, M. A. (2007). Circulation and water mass transformation in a model of the Chukchi Sea. *Journal of Geophysical Research*, *112*, C05025. https://doi.org/10.1029/2005JC003364

Steele, M., Morison, J., Ermold, W., Rigor, I., Ortmeyer, M., & Shimada, K. (2004). Circulation of summer Pacific halocline water in the Arctic Ocean. *Journal of Geophysical Research*, *109*, C02027. https://doi.org/10.1029/2003JC002009

Steinacher, M., Joos, F., Frolicher, T. L., Plattner, G.-K., & Doney, S. C. (2009). Imminent ocean acidification in the Arctic projected with the NCAR global coupled carbon cycle-climate model. *Biogeosciences*, *6*(4), 515–533. https://doi.org/10.5194/bg-6-515-2009

Steiner, N. S., Christian, J. R., Six, K. D., Yamamoto, A., & Yamamoto-Kawai, M. (2013). Future ocean acidification in the Canada basin and surrounding Arctic Ocean from CMIP5 earth system models. *Journal of Geophysical Research: Oceans*, *119*, 332–347. https://doi.org/10.1002/2013JC009069

Stöven, T., Tanhua, T., Hoppema, M., & Bullister, J. L. (2015). Perspectives of transient tracer applications and limiting cases. *Ocean Science*, *11*(5), 699–718. https://doi.org/10.5194/os-11-699-2015

Swift, J., Jones, E., Aagaard, K., Carmack, E., Hingston, M., MacDonald, R., et al. (1997). Waters of the Makarov and Canada basins. *Deep Sea Research Part II*, *44*(8), 1503–1529. https://doi.org/10.1016/S0967-0645(97)00055-6

Tanhua, T., Jones, E. P., Jeansson, E., Jutterström, S., Smethie, W. M., Wallace, D. W., & Anderson, L. G. (2009). Ventilation of the Arctic Ocean: Mean ages and inventories of anthropogenic CO_2 and CFC-11. *Journal of Geophysical Research*, *114*, C01002. https://doi.org/10.1029/2008JC004868

Tanhua, T., Waugh, D. W., & Wallace, D. W. R. (2008). Use of SF_6 to estimate anthropogenic CO_2 in the upper ocean. *Journal of Geophysical Research*, *113*, C04037. https://doi.org/10.1029/2007JC004416

Terhaar, J., Orr, J. C., Gehlen, M., Ethé, C., & Bopp, L. (2019). Model constraints on the anthropogenic carbon budget of the Arctic Ocean. *Biogeosciences*, *16*(11), 2343–2367. https://doi.org/10.5194/bg-16-2343-2019

Uppström, L. R. (1974). The boron/chlorinity ratio of deep-sea water from the Pacific Ocean. *Deep Sea Research and Oceanographic Abstracts*, *21*, 161–162. https://doi.org/10.1016/0011-7471(74)90074-6

van Heuven, S., Pierrot, D., Rae, J., Lewis, E., & Wallace, D. (2011). *MATLAB program developed for CO_2 system calculations*. Oak Ridge, Tenn: ORNL/CDIAC-105b. Carbon Dioxide Inf. Anal. Cent. Oak Ridge Natl. Lab. https://doi.org/10.3334/CDIAC/otg.CO2SYS_MATLAB_v1.1

Wanninkhof, R. (1992). Relationship between wind speed and gas exchange over the ocean. *Journal of Geophysical Research*, *97*(C5), 7373–7382. https://doi.org/10.1029/92JC00188

Warner, M., & Weiss, R. (1985). Solubilities of chlorofluorocarbons 11 and 12 in water and seawater. *Deep-Sea Research Part I*, *32*(12), 1485–1497. https://doi.org/10.1016/0198-0149(85)90099-8

Waugh, D. W., Haine, T. W., & Hall, T. M. (2004). Transport times and anthropogenic carbon in the subpolar North Atlantic Ocean. *Deep-Sea Research Part I*, *51*(11), 1475–1491. https://doi.org/10.1016/j.dsr.2004.06.011

Waugh, D. W., Hall, T. M., McNeil, B. I., Key, R., & Matear, R. J. (2006). Anthropogenic CO_2 in the oceans estimated using transit time distributions. *Tellus B*, *58*(5), 376–389. https://doi.org/10.1111/j.1600-0889.2006.00222.x

Weiss, R. (1974). Carbon dioxide in water and seawater: The solubility of a non-ideal gas. *Marine Chemistry*, *2*(3), 203–215. https://doi.org/10.1016/0304-4203(74)90015-2

Weiss, R., Östlund, H., & Craig, H. (1979). Geochemical studies of the Weddell Sea. *Deep Sea Research Part A*, *26*(10), 1093–1120. https://doi.org/10.1016/0198-0149(79)90059-1

Woodgate, R. (2013). Arctic Ocean circulation: Going around at the top of the world. *National Education of Knowledge*, *4*(8), 8.

Woodgate, R. A., Weingartner, T., & Lindsay, R. (2010). The 2007 Bering Strait oceanic heat flux and anomalous Arctic sea-ice retreat. *Geophysical Research Letters*, *37*, L01602. https://doi.org/10.1029/2009GL041621